Shahrood University of Technology
Iranian Society of Mining Engineering (IRSME)
Journal of Mining and Environment (JME)
journal homepage: www.jme.shahroodut.ac.ir
THOMSON REUTERS
Vol. 11, No. 1, 2020, 77-97.
DOI: 10.22044/jme.2019.8357.1715

Stability Analysis of Salt Cavern Gas Storage Using 2D Thermo-Hydro-Mechanical Finite-Element Software

A. Asgari[1]*, A. Ramezanzadeh[1], S.M.E. Jalali[1], B. Brouard[2]

1. Faculty of Mining, Petroleum & Geophysics Engineering, Shahrood University of Technology, Shahrood, Iran
2. Brouard Consulting, Paris, France

Received 27 April 2019; received in revised form 9 June 2019; accepted 14 November 2019

Keywords

Salt cavern

Stability analysis

Finite element modeling

Sensitivity analysis

Abstract

Ensuring the stability and integrity of underground gas storage salt caverns is a very complicated subject due to the non-linear and time-dependent behavior of rock salts under complicated thermal and mechanical loading conditions. For this reason, pressure and temperature fluctuations in the caverns and their surrounding strata must be integrated into the analysis and the numerical tools that are used for this purpose. LOCAS, a 2D axisymmetric finite-element code, dedicated to the stability analysis of underground salt spaces, was applied to assess the effects of various operating and geometrical parameters on the cavern behavior. In this paper, we aimed to give an overall assessment of the behavior of the salt caverns used for natural gas storage. In this work, some specific loading scenarios were considered first, followed by thorough parametric and sensitivity analyses to reveal the impacts of the geometrical parameters and operational parameters involved on the behavior of salt caverns using the modern stability criteria. The findings showed that the onset of dilation was more likely to happen within the first cavern life cycle when pressure dropped to the minimum level. As for the potential of tension occurrence in the surrounding rock, this is more likely to happen by increasing the number of operation cycles, especially in the upper one-third of the cavern wall. Finally, it was seen that the cavern depth and minimum cavern internal pressure had even more important influences than the others on the salt cavern behavior.

1. Introduction

During the last two decades, the application of gas storage salt caverns has been changed from one-year (seasonal) to high frequency (HF) gas storage cycles (e.g. CAES caverns). The seasonal operation cycles of the caverns is characterized by one withdrawal and re-fill with gas in a year. Seasonal storages are often used as buffers for gas to supply the periods of high demand [1]. The new type of high-frequency (HF) gas storage caverns contains a requirement to obtain at any time in the highest possible withdrawal or re-fill rate for the gas to respond flexibly to the respective gas market situation. Furthermore, growth in the number of gas storage caverns in operation, characterized by high capacity and withdrawal/injection rate, has been dramatically increased within the last decade. As a result of this situation, additional knowledge and understanding of how to design safe storage caverns must be revised. Despite the fact that salt caverns are being regarded as a safe place for storing products, there are many reports about incidents in salt caverns due to the cavern/well stability and integrity issues [2]. These issues have led to many developments in the salt cavern industry, especially from the safety consideration viewpoint.

The salt caverns experience complex mechanical, thermal, and hydraulic processes throughout their life. The state of stresses around a salt cavern depends on the depth of the cavern, primary stress state, internal gas pressure, and injection and

✉ *Corresponding author: aminasgari2010@gmail.com (A. Asgari).*

withdrawal rates. Furthermore, the salt creep behavior and cavern geometry influence stress redistributions during the loading and unloading phases. The thermodynamic processes involved in a gas-storage cavern include (a) the heating and cooling caused by gas compression and expansion, (b) the heat transfer between the gas and the surrounding rock, and (c) the energy changes caused by mass flow into and out of the cavern, which finally lead to temperature changes of the gas in the cavern. Since the salt has a relatively high thermal-expansion coefficient [3], large changes in the gas temperature lead to the creation of significant thermal stresses at the cavern wall [4]. Therefore, the knowledge of the thermo-hydro-mechanical (THM) material behavior of the cavern-product is the main assumption to prove the static stability and tightness of salt caverns [5, 6].

Along with the growth in the cavern industry, significant development steps have been taken in the mechanical analysis of the rock salt behavior. Figure 1 gives an overview of the basic steps within a rock mechanical application for the cavern design. The early constitutive models were used to predict only the steady-state creep deformation of rock salt. These models were suitable for the analysis of crude oil storage salt caverns (see e.g. [7-9]), where no significant stress changes happen. Then with introducing seasonal gas storage caverns, large efforts were focused on constitutive models with the capability of simulating transient and steady-state creep deformation. The main applications of these models were for the caverns with relatively constant internal pressures such as the seasonal gas storage caverns. These types of constitutive models were only applicable for cases that the stress states were below the dilatancy boundary (e.g. BGR, LUBBY2, SUVIC). In this case, damage and dilatation were not considered (see e.g. [10]). During the last two decades, sophisticated concepts based on continuum damage mechanics, especially the damage and healing behavior of rock salt (i.e. continuum damage mechanics, CDM) have been introduced in salt mechanics to predict mainly the HF cavern behavior [11-14]. After that, the views on the mechanical behavior of rock salts have changed from a ductile manner without micro-fissuring to open and close inter-crystalline micro-fractures upon reaching a certain level of stress intensity and loading rate [5, 15]. Table 1 depicts the most advanced constitutive models, and numerical codes have been recently used in the salt cavern industry.

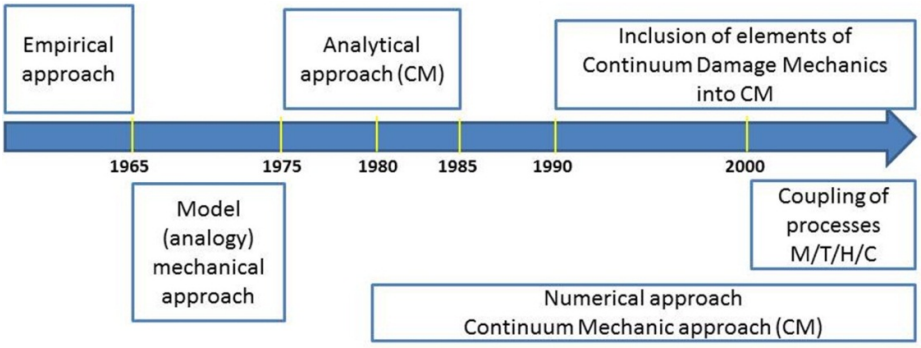

Figure 1. Significant development steps in the mechanical analysis of rock salts [16].

Table 1. Most advanced constitutive models and numerical codes (Modified after [13]).

Constitutive model	Numerical code
Composite Dilatancy Model (CDM)	FLAC3D
Günther/Salzer Model	FLAC, FLAC3D
KIT Model	ADINA
Lubby-MDCF Model	FLAC3D, LOCAS
TUB Ssalt Model	FLAC3D, ANSYS
MD Model	Sierra Mechanics Code Suite, FLAC, FLAC3D, LOCAS

The mechanical behavior of rock salts as a polycrystalline material has been extensively studied in terms of the macro-structure (viscoelastic, viscoplastic, and damage phenomena) and micro-structure scales. In the micro-structure scale, the dislocation mechanisms of defects in the crystalline structure of rock salts is the main attribute process involved in salt rock

deformation. There are various shapes of defects in the lattice arrangements of atoms in rock salt crystal (e.g. 0D, 1D, 2D and 3D). Hirth and Lothe (1982) have described these imperfections or defects as point, linear, planer, and bulk defects [17]. Regarding the salt caverns and based on the combination of these defects, three major dislocation mechanisms including dislocation glide, dislocation climb, and solution precipitation have been identified to be responsible for rock salt behavior in the vicinity of cavern walls. These mechanisms are typically presented in a deformation map (Figure 2). It should be stated that the interaction between these mechanisms is complicated, which is further described in Section 2.2.

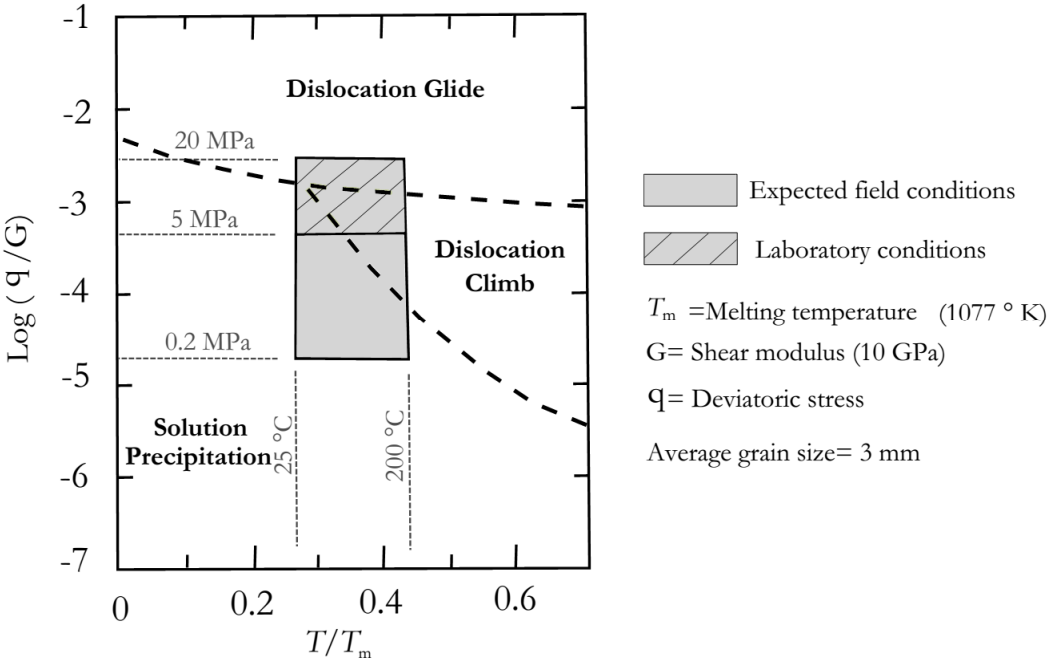

Figure 2. Deformation mechanism map of rock salts [18].

The macro and micro-structure studies provide a basis for developing the rock salt advanced constitutive models. Among these advanced constitutive material models, the Multi-mechanism Deformation (MD) model was the first model that was developed on the basis of the deformation mechanism map [19]. This model is widely used to describe the time-dependent mechanical behavior of salt caverns [13, 20-22]. In the last ten years, the MD model has been extended greatly and a number of modified versions of MD model such as IUB-MDCF and LUBBY-MDCF have been suggested [11, 23-25]. Also this model has been extensively used in the research works. In the recent works, Costa *et al*. (2018) have used the MD model to investigate an experimental study of a salt mine gallery [26] and Pedro *et al*. (2018) have derived benefits from the MD model to construct their own EDMT formulation [27]. For this work, the basic MD model was applied. In this model, the total creep strain rate is a summation of three terms that are associated with a specific creep deformation mechanism, namely (a) dislocation climb mechanism, (b) micro-mechanistically undefined mechanism for low stresses, and (c) dislocation glide mechanism.

Besides using the proper and task-oriented constitutive material model, the numerical software that the model is implemented to it should be able to compute cavern thermodynamics and to calculate the thermo-elastic stresses that are triggered by cycles in the vicinity of cavern wall and to perform fully coupled thermal, hydraulic, and mechanical computations at the same time. In other words, in any software computations for gas storage salt caverns, the following criteria should be considered: (a) salt creep using advanced constitutive laws, (b) heat flux to or from the rock mass and heat exchange between gas and brine, (c) real gas thermodynamics, and (d) mechanical and thermal expansion/contraction of the cavern products [28].

Regarding the rock-mechanics computations related to salt caverns, there are a limited number

of numerical codes available commercially. The two well-known FDM and FEM programs FLAC3D and ABAQUS, respectively, are the most used worldwide [8] but they suffer from some important limitations when working with salt caverns [28]. Firstly, a very limited number of suitable constitutive laws for rock salt are available in these software packages. Secondly, these software packages are unable to calculate the cavern thermodynamics, salt geomechanics, and hydraulics simultaneously, which are prerequisites for salt cavern computations. Thirdly, standard embedded mesh generators (such as FLAC) may not be suitable for the gas-cavern problems, where very fine meshes are required. In this work, we considered the MD constitutive model incorporated into a FEM computer 2D axisymmetric software program, entitled "LOCAS". This software package has been dedicated to salt caverns. LOCAS is able to compute cavern thermodynamics and to calculate the thermo-elastic stresses that are triggered by cycles and to perform two-way coupled thermal, hydraulic, and mechanical computations at the same time. The LOCAS software has been extensively used for various short-term and long-term salt cavern stability computations such as cavern abandonment [29-31], seasonal gas storage cavern [32], HF gas storage cavern [33], and even in extreme cases (i.e. cavern blowout) [34].

Dealing with the analysis of salt caverns, the stability criteria are very important to assess the stability and integrity of caverns. Several authors have addressed general demands and technical safety recommendations for salt cavern design (see e.g. [4, 15, 28, 35]). Costa *et al*. (2015) [21] have used horizontal and vertical displacements and effective stress on the cavern wall to assess the cavern stability. In a research work carried out by Gährken *et al*. (2018), they evaluated Lode angle influence on stability analysis of a salt cavern and modified the TUB Ssalt constitutive model. Li *et al*. (2018) [8] have applied the stress-to-strength ratio at the cavern wall and in the pillar area and the effective strain increment at the rock salt cavern contour as their design criteria for underground salt cavern storage. The following stability criteria were provided by Brouard *et al*. (2011) [35, 36], which were regarded in this work to discuss the cavern mechanical and hydraulic conditions:

- no or small dilatant zone in the rock mass and at the vicinity of cavern;
- no or small tensile zone in the rock mass and at the vicinity of cavern;
- no or limited effective tensile zone in the rock mass and at the vicinity of cavern;
- limited cavern volume loss and volume loss rate (up to e.g. 1% per year)

The objective of this work was to present an assessment of the thermo-mechanical behavior of seasonal and HF salt caverns through a sensitivity analysis. Also thermo-mechanical coupled calculations were performed for a seasonal baseline model to investigate the effects of various operating conditions such as the minimum and maximum pressure, and cycle number and period on cavern stability and integrity. We also considered the effect of cavern geometry and cavern depth. A sensitivity analysis was used to account for the interactions among so many processes, properties, and parameters, plus uncertainty of parameter values. Thus thorough sensitivity analyses of gas caverns with respect to cavern geometry (cavern depth, shape, and volume) and operation pattern (max/min pressure, cycle number, cycle period, and gas injection temperature) were employed to investigate the impacts of these parameters on the salt cavern behavior.

2. Salt Cavern simulation

In order to evaluate the critical model parameters and assess the impact that they have on the numerical solution, a modeling effort was organized in the following steps:

- Construction of a baseline model,
- Evaluating the stability criteria,
- Stability analysis of the cavern baseline model,
- Sensitivity analysis of the geometrical and operational factors involved in the stability of the salt formation in a particular area around the cavern body (i.e. casing-shoe area).

This issue will be further discussed in Section 2.2.

2.1. Baseline model for gas storage salt cavern

2.1.1. Geological Structure

A stratigraphy was generated for the simulations according to a typical salt-dome stratigraphy. The geologic formation includes two salt and overdurden layers that lie from the ground surface to 2200 m depth (Table 2).The overlying sediments were modeled as an elastic-behaving material. A schematic representation of the baseline cavern design is shown in Figure 3. The

initial state of stress was assumed to be isotropic and equal to the weight of the overburden. A ground surface temperature of 25 °C and a geothermal gradient of 1.87×10^{-2} /m were assumed [37]. Also an isotropic *in situ* state in the salt was assumed in this study, where all the three principal stresses were equal.

Table 2. Stratigraphy and geomechanical properties of the layers used for simulations.

Layer No.	Type	Thickness (m)	Density (kg/m^3)	Young's modulus (GPa)	Poisson's ratio
1	Overburden	200	2600	40	0.35
2	Salt	2000	2200	30	0.25

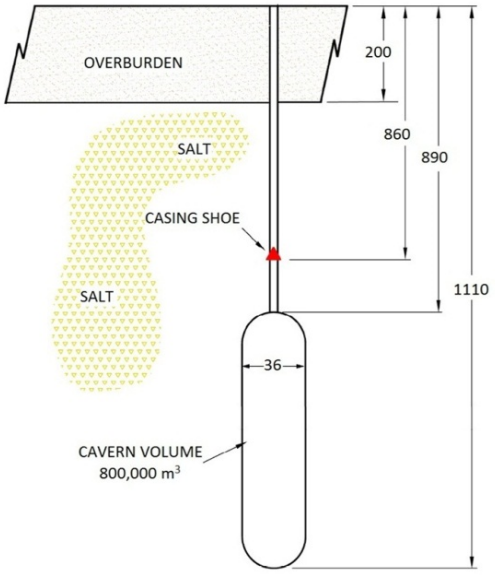

Figure 3. A schematic representation of the baseline cavern model (modified after [38]).

2.1.2. Geomechanical characteristics and constitutive law of salt rock

The MD model was applied to describe the creep deformations using the FEM software LOCAS to generate the model and perform the simulation. The deformation rate of the salt can be decomposed into the thermal expansion, elastic deformation, and inelastic deformation. The inelastic deformation is stress-, temperature-, and rate-dependent. It comprises both the viscoplastic (creep) and brittle components, with the viscoplastic component usually dominating in the range of stress and temperature expected in the salt surrounding the cavern model.

Two differential rate equations comprise the M-D model: the strain-rate equations that give the viscoplastic strain rates, and the evolutionary equation that gives the rate of change of an internal variable. As indicated by (1), the steady-state creep rate $\dot{\varepsilon}_s$ based on the M-D model is composed of three terms. Each term is associated with a different creep mechanism as follows:

$$\dot{\varepsilon}_{ij}^{vp} = {\partial \sigma_e}/{\partial \sigma_{ij}} F \dot{\varepsilon}_s \qquad \dot{\varsigma} = (F-1)\dot{\varepsilon}_s \qquad \dot{\varepsilon}_s = \sum_{i=1}^{3} \dot{\varepsilon}_{s_i} \tag{1}$$

where $\dot{\varepsilon}_s$ is the steady-state strain rate for the creep mechanism i.

$$\dot{\varepsilon}_{s_i} = A \exp(-Q_i/RT)\,(\sigma_e/\mu)^{n_i} \qquad i = 1 \text{ or } 2 \tag{2}$$

$$\dot{\varepsilon}_{s_3} = [B_1 \exp(-Q_1/RT) + B_2(-Q_2/RT)].\sinh[q(\sigma_e - \sigma_0)/\mu]\, H(\sigma_e - \sigma_0)$$

$$F = \begin{cases} \exp\left[\Delta(1-\frac{\varsigma}{\varepsilon_t^*})^2\right] & for\ \varsigma < \varepsilon_t^* \\ 1 & for\ \varsigma = \varepsilon_t^* \\ \exp\left[-\delta(1-\frac{\varsigma}{\varepsilon_t^*})^2\right] & for\ \varsigma > \varepsilon_t^* \end{cases} \tag{3}$$

$$\varepsilon_t^* = K_o \exp(c_{MD}T)\,(\sigma_e/\mu_{MD})^{m_{MD}} \qquad \Delta = \alpha_w + \beta_w \log(\sigma_e/\mu_{MD})$$

and

$\dot{\varepsilon}_{ij}^{vp}$	viscoplastic strain-rate tensor
$\sigma_e = \sqrt{3J_2}$	effective stress
$J_2 = \frac{1}{2}s_{ij}s_{ji}$	
$s_{ij} = \sigma_{ij} - \delta_{ij}\sigma_m$	deviatoric stress tensor
$\sigma_m = \frac{1}{3}\sigma_{kk}$	mean stress
σ_{ij}	stress tensor
δ_{ij}	Kronecker delta
ς	internal variable
T	absolute temperature
$H(x)$	Heaviside function
μ_{MD}	a normalizing constant equal to the shear modulus ($1.7985 \times 10^6\ psi = 12.4\ GPa$)

$A_1, A_2, B_1, B_2, Q_1, Q_2, n_1, n_2, q, \sigma_0, \delta, K_0, \mathrm{c}, \mathrm{m}, \alpha_w, \beta_w$ are the experimentally determined parameters. The first and third mechanisms ($\dot{\varepsilon}_{s_1}$ and $\dot{\varepsilon}_{s_3}$) are the dislocation climb and dislocation glide, respectively, and the second mechanism ($\dot{\varepsilon}_{s_2}$) is referred to as the undefined mechanism.

The MD parameter and also thermal parameter Table 3. The thermal properties for the rock salt are used to perform the thermo-mechanical calculations in the surrounding cavern formation. Table 4 gives the typical thermal properties of the salt and natural gas, respectively, assumed for the simulations [31, 35].

2.1.3. Cavern geometry, meshing, and boundary condition

The results presented in this paper are based on the simulation of an 800,000 m^3 (5 MMbbls) values for the rock salt are given in cavern. The cavern is capsule-like in shape, 220 m height, and has a maximum radius of 36 m. Table 5 gives the cavern geometry and meshing parameters. The distribution and size of meshes used for the numerical computation is shown in Figure 4. The mesh size and its distribution around the cavern has a significant effect on the numerical result [35, 39]. For this study, a very fine mesh in the vicinity of cavern wall was regarded (say 0.5 m).

Table 3. Considered mechanical and thermal parameters for the rock salt [40].

Munson-Dawson model parameters				Thermodynamic parameters		
	Parameter	Unit	Value	Parameter	Unit	Value
Steady-state creep	A	/MPa^n-yr	0.74	Thermal capacity	J/kg-K	921
	n	−	5	Thermal diffusivity	$\times 10^{-6}$ m²/s	3
	Q/R	K	5032			
Transient creep	m	−	3	Thermal Conductivity	W/m-K	6.08
	α_w	−	-13.2			
	β_w	−	-7.738	Thermal expansion coefficient	$\times 10^{-4}$ /°C	4
	K_0	/MPa^m	7×10^{-7}			
	δ	−	0.58			
	c	/K	9.02×10^{-3}			

Table 4. Thermodynamic properties of natural gas.

Parameters	Unit	Value
Temperature reference	K	293.15
Pressure reference	atm	1
Density	kg/m^3	0.67
Thermal capacity C_p	J/kg-K	2168.6
Thermal capacity C_v	J/kg-K	1683
Ratio C_p/C_v	−	1.296
Dynamic viscosity	$\times$1E10^{-5} Pa.s	1.025

Table 5. Cavern geometry and meshing parameters.

Baseline geometry parameters		Meshing parameters	
Cavern shape	Capsule	Elements	13777
H:D ratio	3	Nodes	7220
Cavern volume (m^3)	8×10^5	Height (m)	2200
Cavern max. radius (m)	36	Width (m)	1000
Average cavern depth (m)	1000	Average distance between nodes on wall (m)	0.5
Top cavern depth (m)	890		
Casing-shoe depth (m)	860		

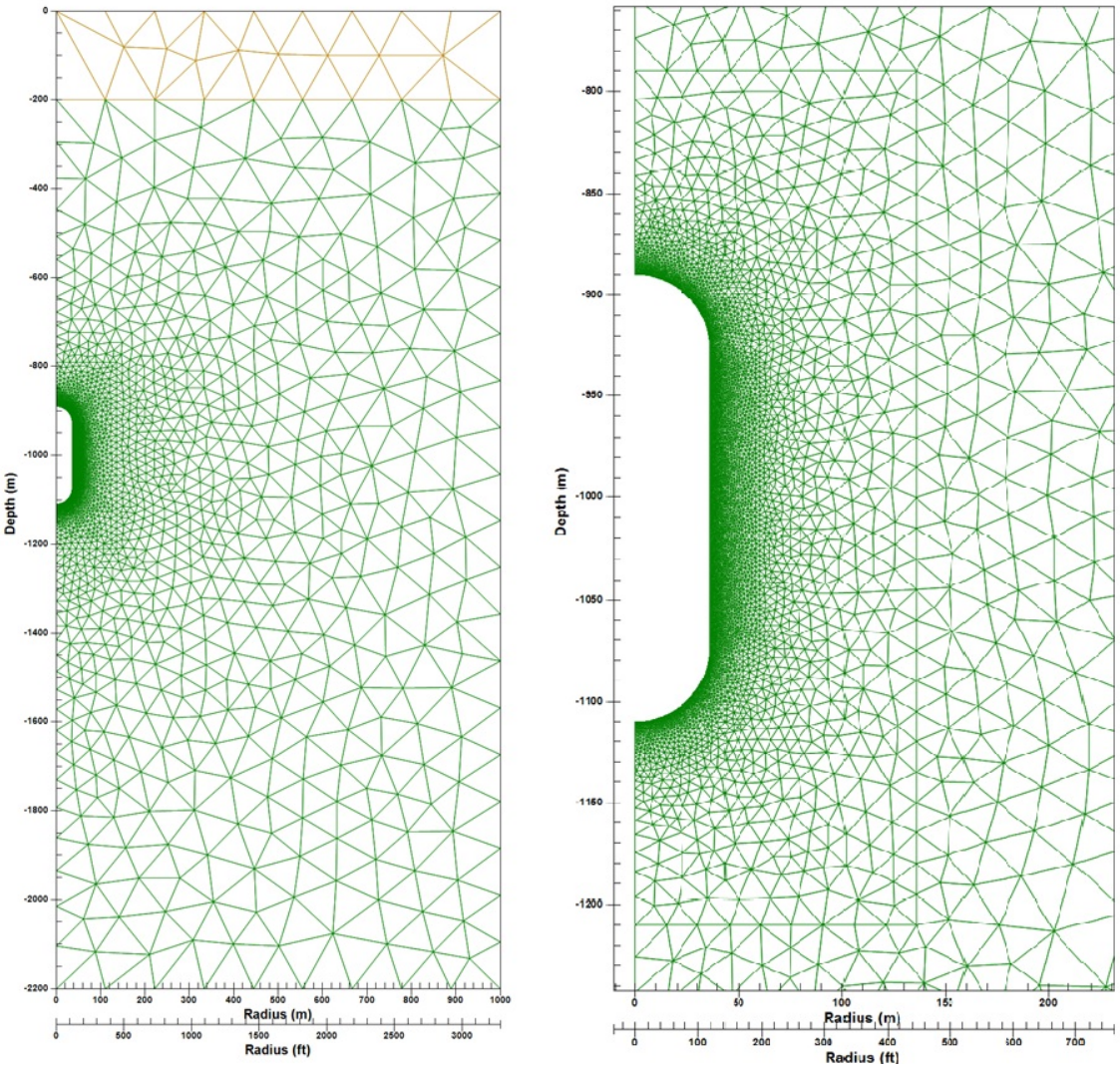

Figure 4. Mesh used for the numerical analysis.

The boundary condition applied along the right side of the model was a geostatic pressure (see Figure 5). The model represents a single cavern in a semi-infinite salt dome, where the effects from the other caverns are neglected. Also a geothermal gradient boundary is assumed on all the four boundaries of the model. As the mechanical boundary conditions, the upper surface was free (zero stress), while the bottom and the other lateral sides were fixed in the perpendicular direction.

2.1.5. Operational history for gas storage cavern

The baseline annual gas-storage cycle (cavern pressure history) is presented in Figure 7. In all of the simulations, the casing seat was assumed to be 30 m above the cavern top. All of the gas-storage simulations were preceded by a cavern leaching phase (2 years) and a debrining phase (1 year). During the creation period, the cavern pressure decreases from geostatic (22.4 MPa) to halmostatic (pressure of a brine column) (11.5 MPa); during debrining, the cavern pressure reached 16.5 MPa (i.e. a pressure gradient of 0.85 psi/ft at the casing-shoe depth), after which the cavern could be operated as storage for natural gas (see Figure 6).

Each of the turns in the cycle includes withdrawal of the working gas over a period of 150 days, followed by injection of the working gas over a 215-day period. For the baseline cavern, with a minimum casing-seat pressure gradient of 0.20 psi/ft (4.5×10^{-2} MPa/m), the pressure at the cavern top is 4.5 MPa. At the maximum baseline casing-seat pressure gradient of 0.85 psi/ft, the pressure at the cavern top is 16.5 MPa. In order to achieve a nearly steady-state thermal cycle in the

cavern, the annual gas cycle was repeated continuously for 10 years. Also the injection temperature of the gas was assumed to be 37 ˚C.

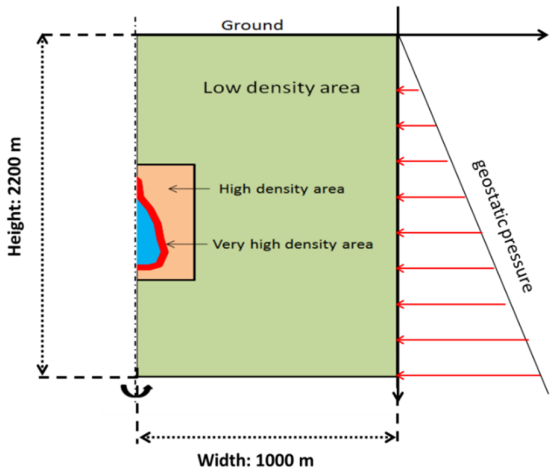

Figure 5. Boundary condition applied for the baseline model.

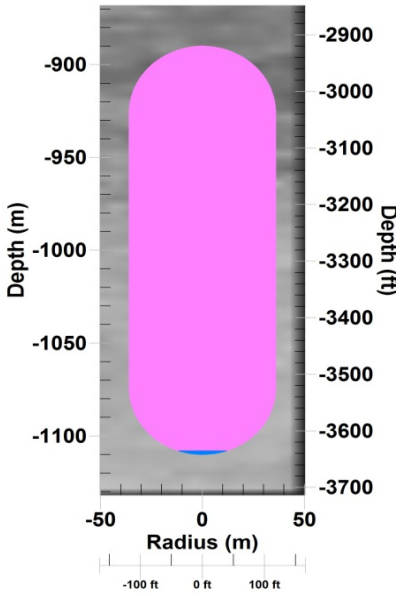

Figure 6. A schematic representation of the cavern and stored product at the end of the debrining stage.

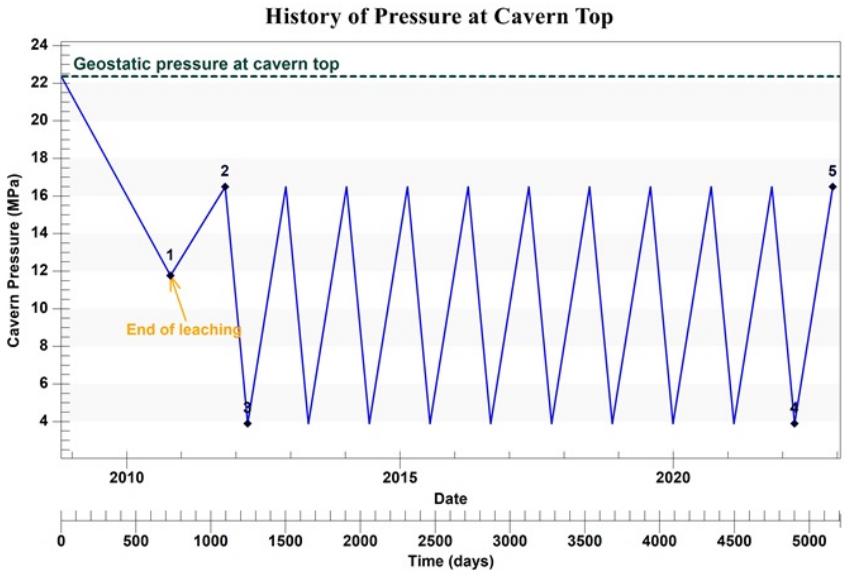

Figure 7. Cavern pressure history for baseline model; (1) end of leaching/start of debrining, (2) end of debrining/start of operation/first maximum pressure, (3) first minimum pressure, (4) tenth minimum pressure, and (5) tenth maximum pressure.

2.2. THM coupling for gas storage cavern

Beside the purely mechanical processes (M), thermal processes (T), and hydraulic processes (H), an adequate and accurate numerical computation requires applying coupled thermo-hydro-mechanical (THM) coupling for modeling salt caverns under cyclic loading [30, 41]. For example, in an extreme case (i.e. cavern blowout) where the cavern pressure decreases suddenly to the atmospheric pressure, considering the full coupling of the system (i.e. the Fanno flow in the well, heat flux from the rock mass, gas water condensation, and heat exchange between gas and brine in the cavern) is necessary [42]. In the THM coupling concept, the mechanical, hydraulic, and thermal field in a plausible as well as compatible manner allow for interaction [43]. There is a great complexity in THM simulation of salt caverns. Firstly, the THM parts interact and influence the others in a complex manner. Secondly, these parts

are not in the same spatial and temporal scales. Thirdly, some of the couplings between these parts are "one-way coupling", while the others are "two-way coupling" [44]. An example for a "one-way coupling" is the interrelation between the brine temperature and brine pressure; while the brine temperature changes the results in the brine pressure change, the pressure change in brine does not cause a significant brine temperature change. An example for "two-way coupling" is the inter-relation between the salt creep and the brine pressure, where salt creep causes brine pressure change and brine pressure change impacts salt creep.

In this work, a fully coupled THM numerical simulation of gas storage cavern was conducted under various cycling scenarios using the LOCAS software, which included (a) coupled thermodynamics of gas in the cavern, (b) coupled time-dependent thermo-mechanic of rock salt surrounding the cavern, (c) heat transfer between gas in the cavern and the host rock, and (d) heat transfer between gas in the cavern and brine at the bottom of the cavern.

2.3. Stability criteria for gas storage cavern

The simulations focus on the operational performance and cavern stability factors, specifically, cavern volumetric closure, salt dilation, and stress states in the host rock. When working with cycling loading and cavern stability, the onset of tensile stresses and salt dilation at the cavern wall must be considered. The tensile strength of salt is low, and large tensile stresses lead to roof or wall spalling. For this reason, the tangential tensile zones must be avoided (i.e. $\sigma_{tt} < 0$). In addition, the effective stress at the cavern wall must be negative (i.e. $\sigma_{tt} + P < 0$, where P is the cavern gas pressure). The cavern volume loss and subsidence are closely related. The cavern volume-loss rate is typically limited to 1% per year.

When shear stresses are large (compared to the mean stress), salt micro-fracturing and dilation take place, which leads to an increase in permeability and a loss of rock strength [35]. For this reason, a large dilatant zone must be avoided. Salt dilation is a term used to describe the transition in the deformation behavior of salt from isochoric (constant volume) creep to a combination of creep and the volume-increasing deformation process of salt-crystal microfracturing and grain-boundary loosening.

The salt dilation criteria from analytic solution viewpoint can be categorized into two classes: (a) invariant-based criterion (see Figure 8) and (b) stress-based criterion (see Figure 9). The invariant-based criterion including stress invariant and stress-based criterion includes minimum principal stress and effective stress. Also these dilation criteria can be classified into linear [45, 46] and non-linear forms [40, 47-49]. The most used dilation criteria in salt cavern industry among others have been prepared by Spiers et al. (1988), Ratigan et al. (1991), Hunsche (1993), Thorel et al. (1996), Hatzor and Heyman (1997), and De Veries (DV) (2005) [40, 45-49].

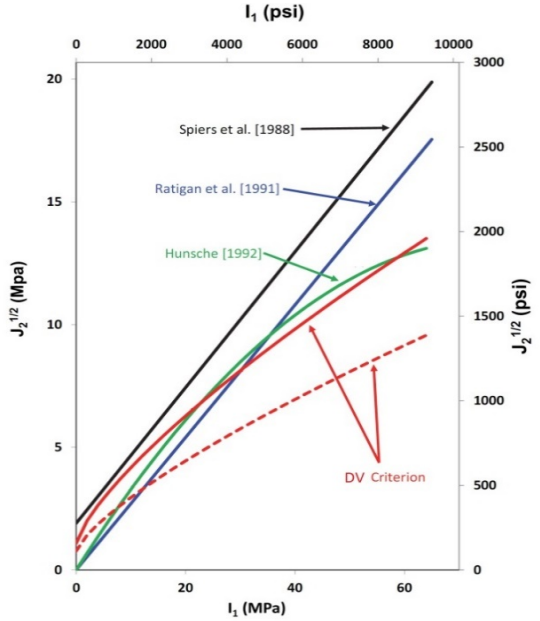

Figure 8. Comparison of invariant-based dilatant boundary criteria in $J_2^{0.5} - I_1$ space [42].

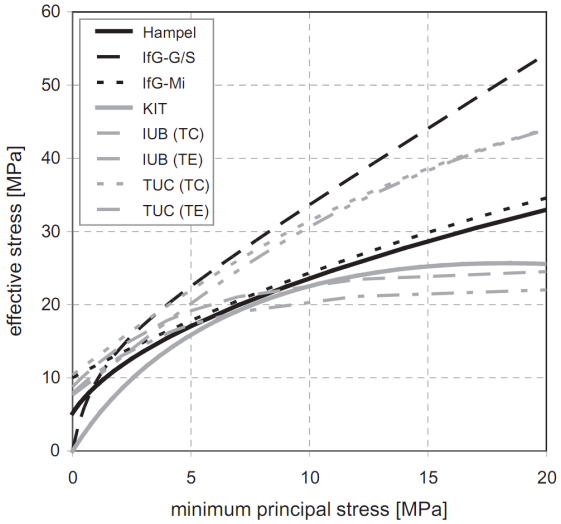

Figure 9. Comparison of stress-based dilatant boundary criteria in $\sigma_{eff} - \sigma_{min}$ space, TC: triaxial compression, TE: triaxial extension [50].

In this work, the DeVries (DV) criteria [40] were used to quantify the regions of dilatant salt. The damage potential criterion relates three stress invariants: the first invariant of the Cauchy stress tensor (I_1),the second invariant of the deviatoric stress ($\sqrt{J_2}$), and the Lode angle (θ) that is defined as:

$$\sqrt{J_2} < \sqrt{J_{2\,dil}} = \frac{D_1(\frac{|I_1|}{sgn(I_1)\sigma_0})^m + \bar{T}_0}{\sqrt{3}\cos\theta - D_2\sin\theta} \quad (4)$$

where $\sigma_0 = 1$ MPa is a dimensional constant, $\bar{T}_0$ is the unconfined tensile strength of salt, θ is the Lode angle, and (D_1, D_2, m) are the salt parameters. Dilation appears when the Factor of Safety (*FOS*) falls below 1:

$$FOS = \sqrt{J_{2\,dil}} / \sqrt{J_2} \quad (5)$$

Table 6 gives the DV dilation criteria parameters selected for this work.

3. Stability analysis of cavern baseline model

With increase in the number of storage cycles, when the gas temperature is higher or lower than the in-situ salt temperature, heat will be transferred between the cavern and the surrounding salt so that the average cavern temperature changes to obtain a balance with the geothermal temperature. From Figure 10, it can be concluded that the effect of decreasing pressure (withdrawal phase) on the cavern gas temperature is greater than increasing pressure (injection phase), resulting in more thermal stress being induced in the withdrawal phase. A 12.5-MPa pressure change between the max/min cavern gas pressures results in a 21 ˚C temperature change within the cavern.

As shown in Figure 11, the cavern volume generally decreases over time but with a periodic increase during the gas injection interval. The average cavern volume loss during the cavern simulation was about 0.17% per year, which satisfied the criteria.

Table 6. Parameters for the DeVries dilation criteria [37].

Parameters	Unit	Value
T_0	MPa	1.95
m	-	0.693
D_1	MPa	0.773
D_2	–	0.524

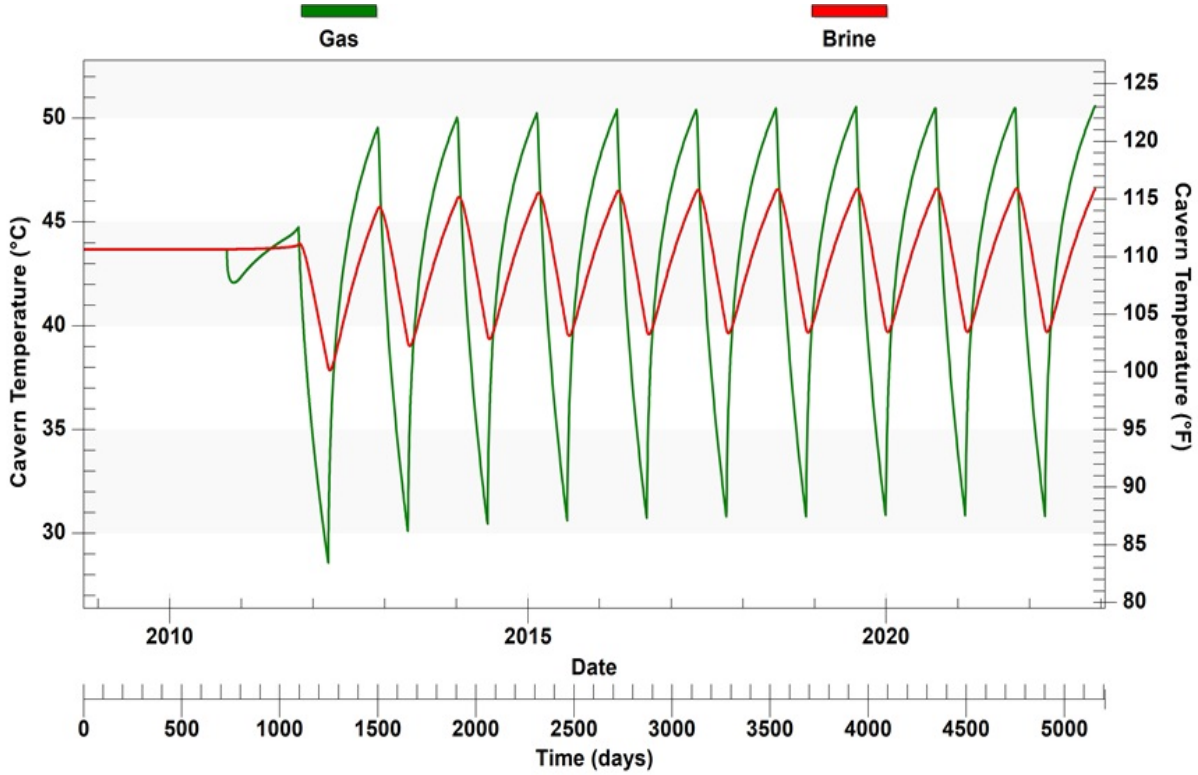

Figure 10. Computed evolution of cavern temperature for gas and brine.

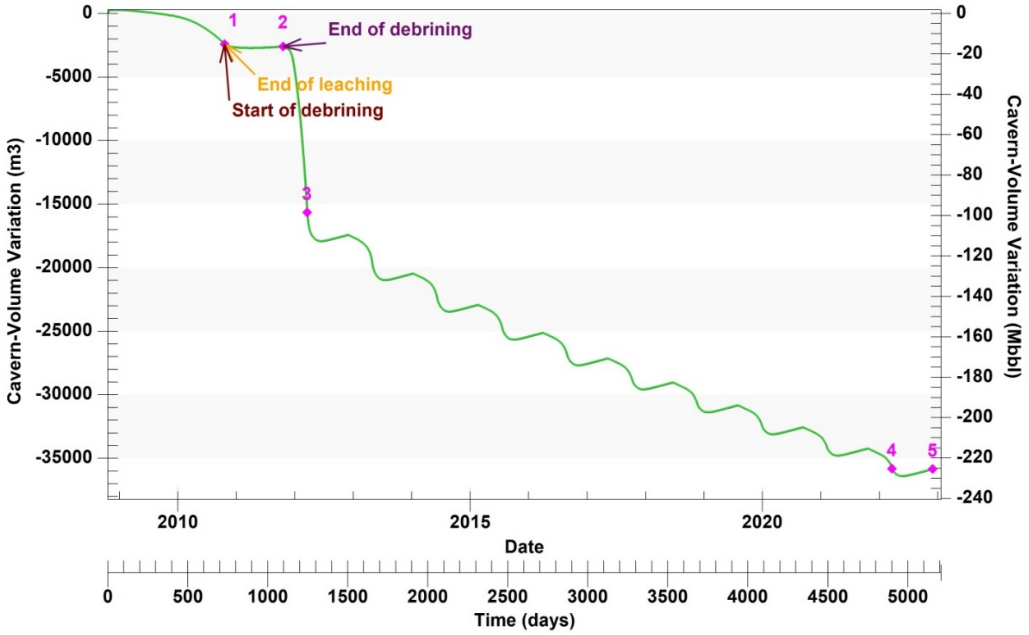

Figure 11. Evolution of cavern volume.

3.1. Stability analysis along cavern wall

Figure 12 shows the stress distribution in terms of the least principal stress along the cavern wall for the selected times in the cavern history (see Figure 7). The area most vulnerable to the tensile failure is the cylindrical part of the cavern, where the cavern pressure is at its lowest value. The maximum principal stress at this part of cavern reaches -0.5 MPa (the sign of the compressional pressure is negative in this work) at the10th minimum pressure. Nevertheless, the stresses remain compressive at the cavern wall during the cavern life. It can be observed that at the end of leaching and debrining, and during the first minimum pressure, the distribution of the least-compressive stress at the cavern wall is uniform. After the 1st minimum pressure, the tensile stress distribution on the cavern wall is almost non-uniform and increases with increasing cycles.

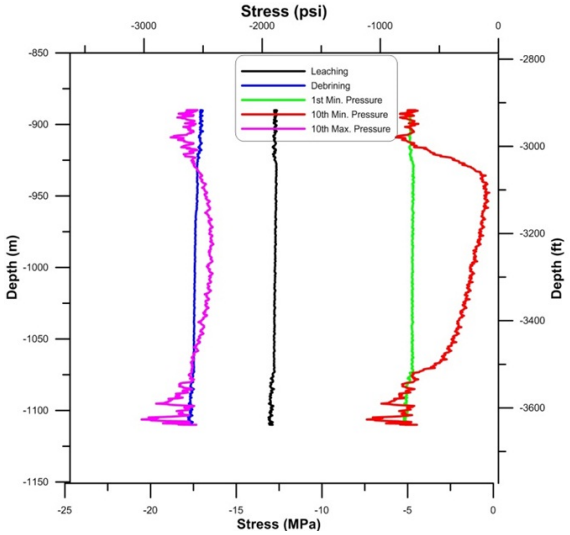

Figure 12. Least principal-stress distribution along the cavern wall.

Figure 8 shows the stress distribution in terms of the effective stress along the cavern wall for the selected times in the cavern history (see Figure 7). The area most vulnerable to the effective tensile failure is at the bottom of the cavern roof at a depth of 950 m at the time at which the cavern

pressure is at its lowest value. It can be observed that at the end of leaching and debrining, and during the first minimum pressure, distribution of the effective stress at the cavern wall is uniform and in a compressive state. As shown in Figure 12, the area most vulnerable to the tensile failure is the cylindrical part of the cavern, where at the time at which the cavern pressure is at the lowest value, the cavern pressure is also at its lowest value. At the 10th minimum pressure, the middle part of the cavern wall is in its tensile mode, which means that the developing tensile area at the cavern wall is most likely when the number of storage cycles increases. It should be noted that during the cavern life, the state of effective stress remains compressive in the upper and lower spherical parts of the cavern wall. This suggests that tensile stresses are more likely to develop in the vicinity of the zones, where a flat or non-convex wall is present.

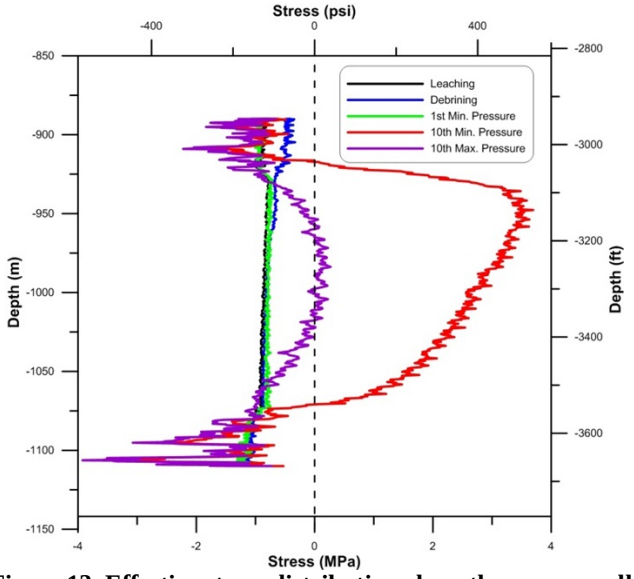

Figure 13. Effective stress distribution along the cavern wall.

Figure 14 shows the evolution of the stress state as a function of shear stresses and mean stresses (invariants plane). The state of stress can be computed at the cavern wall at a 1000–m depth (red points in Figure 14). The state of stress is "normal", except during the short periods of times when the considered point at the cavern wall experiences dilatancy. Another computation is performed for the other parts of the cavern wall, roof, bottom, and casing-shoe area (green points in Figure 14). When comparing these points, it can be observed that dilatancy is more likely to happen at the middle height of the cavern wall (1000-m depth).

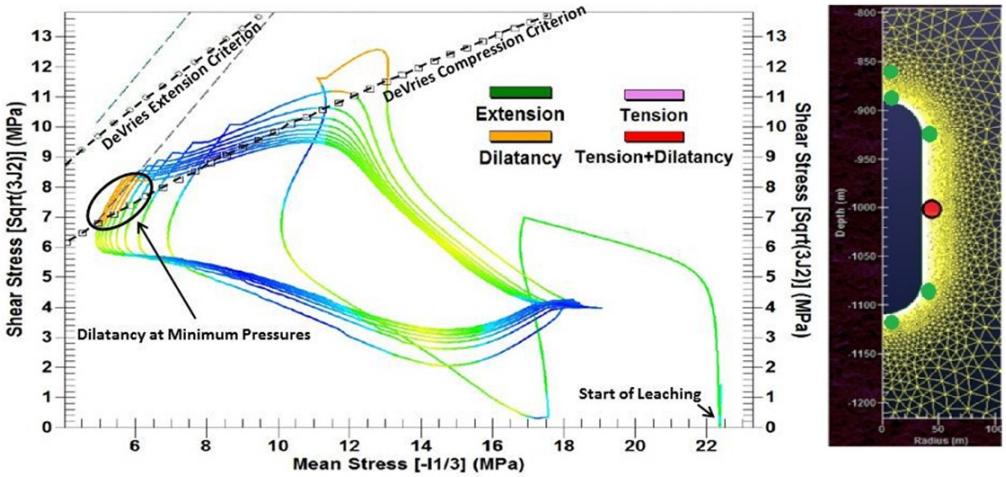

Figure 14. Evolution of stress state at the cavern wall of 1000-m depth (red points).

3.2. Stability analysis along radial direction

Figure 15 shows the radial stress distribution in terms of the least-compressive principal stress along the radial direction at the middle height of the cavern (i.e. at a 1000-m depth) for the selected times in the cavern history (see Figure 7). As shown in this figure, when the cavern pressure is in its minimum state, the least-compressive principal stress at the vicinity of the cavern reaches its maximum (i.e. tensile stress). Also distribution of the least-compressive stresses shows that the thickness of stress distributed zone is approximately $\Delta r = 10\,m$.

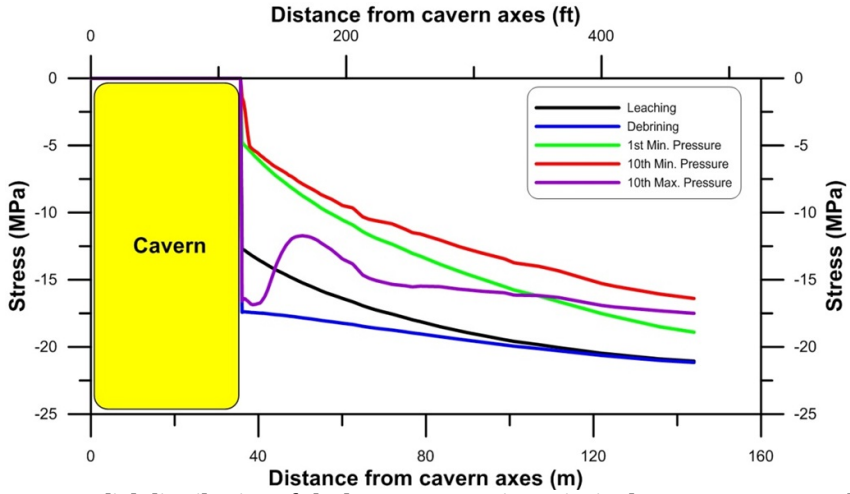

Figure 15. Radial distribution of the least-compressive principal stress at a 1000-m depth.

Figure 16 illustrates the radial stress distribution in terms of the effective stress along the radial direction at mid-height (1000 m) for the selected times in the cavern history (see Figure 7). Similar to the least-compressive principal stress criteria, the most critical condition occurs when the cavern is in its minimum pressure period but the magnitudes of stresses are more tensile. Also by comparing the effective stresses at the first and 10^{th} minimum pressure, it can be seen that the stresses have been more compressive with respect to time.

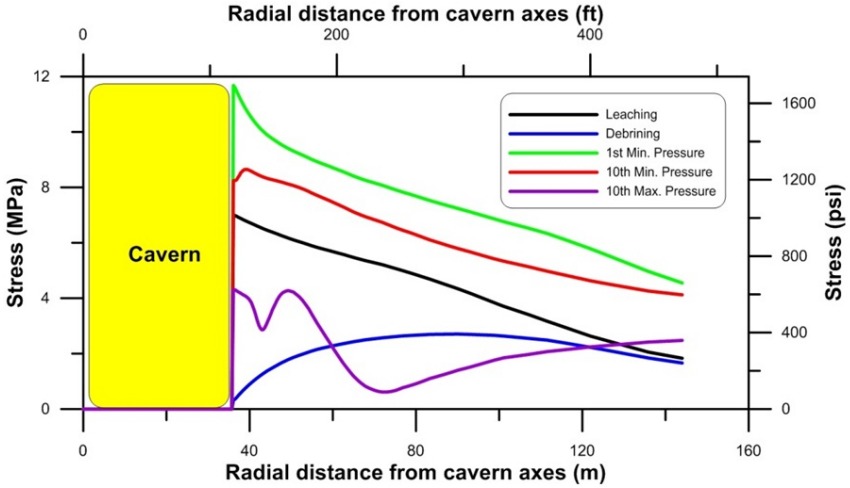

Figure 16. Effective stress distribution along the radial direction at 1000 m.

Figure 17 illustrates the salt dilation potential considering the DV criteria along the radial direction at cavern mid-height FOS plotted for the selected times in the cavern history. During the cavern life, no dilation occurs, and the minimum FOS is larger than 1. In the distance of two times the cavern radius from the cavern wall, FOS for the first and 10th minimum pressures is less than 2. Also along the radial direction in the surrounding salt, FOS for the 10th minimum pressure is greater than the first minimum pressure (i.e. FOS 10th > FOS 1st).

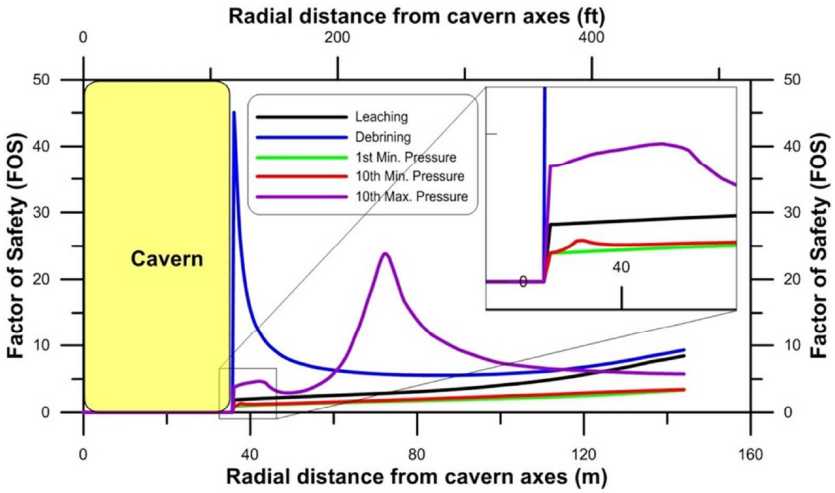

Figure 17. Dilation states along the radial direction at 1000-m depth as FOS.

3.3. Stability analysis along vertical direction

Figure 13 shows the vertical stress distribution along the cavern axis above the cavern in terms of the least-compressive principal stress for the selected times in the cavern history. Figure 14 shows the potential of dilation (DV criteria) of salt rock along the cavern vertical axis as FOS. When the pressure is minimum in the cavern, the confining stress is low and the deviatoric stress is high; therefore, the risk of dilation is maximum (FOS near 1). Conversely, there is no risk of dilation in the salt mass when the cavern pressure is maximum.

3.4. Stability analysis at casing-shoe area

The variations in the least-compressive stress, effective stress, and dilation potential in the casing-shoe area are shown in Figure15, Figure 16 and Figure 18, respectively. As shown in Figure 12, the least-compressive stress variations increase as the number of cycles increases. The least-compressive stress in the cavern is highest at the 10th minimum pressure. As shown in Figure 16, the tensile effective stresses are likely to develop at the casing-shoe area at the time at which the cavern pressure experiences a large pressure increase. The effective tensile stresses due to excessive temperature changes must be avoided, as these can lead to macroscopic fractures at the cavern wall due to the low tensile strength of rock salt. Also the effective stress variations increase as the number of cycles increases (it is the highest at the 10th maximum pressure cycle).

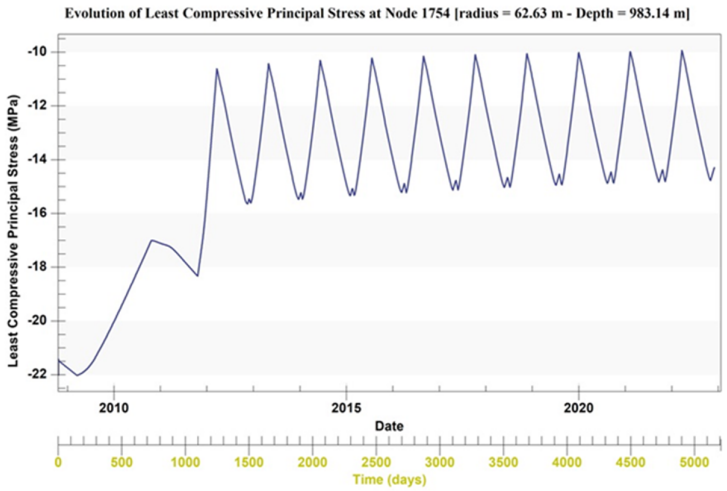

Figure 18. Evolution of least-compressive principal stress at the casing-shoe area.

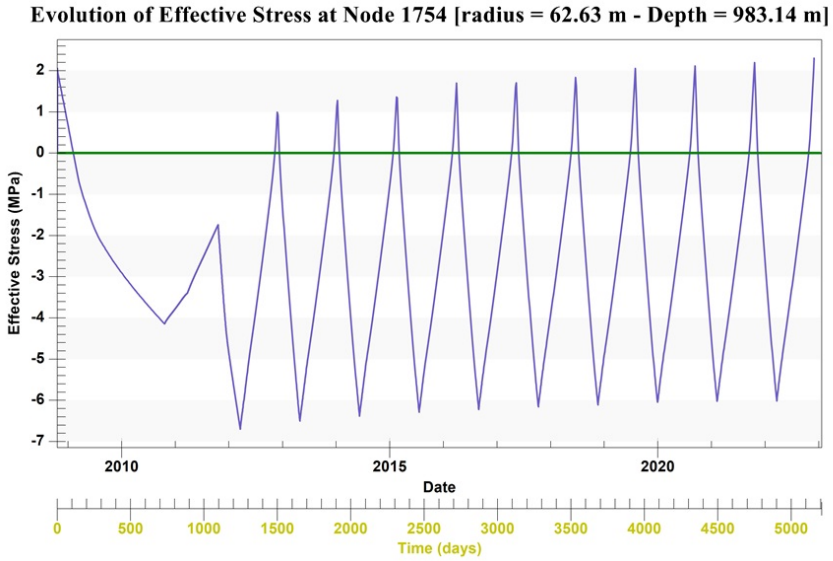

Figure 19. Evolution of effective stress at the casing-shoe area.

The last parameter evaluated was dilation potential. Figure 20 depicts the evolution of dilation potential (DV criteria) at the casing-shoe area. Dilation-potential variations decrease as the number of turns increases. Thus it can be said that dilation-potential is likely to develop at the casing-shoe area during the beginning of the cavern life cycles at the time at which the cavern pressure drops to its minimum level.

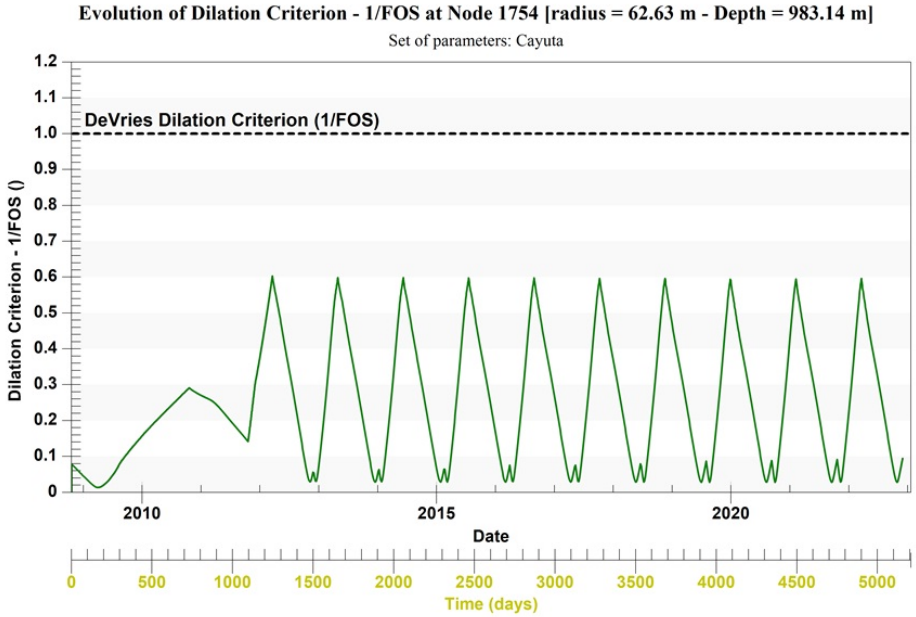

Figure 20. Evolution dilation potential (DV criteria) at the casing-shoe area.

4. Sensitivity analysis for cavern baseline model

Table 7 presents the baseline set of typical operational and design parameters chosen for the sensitivity analysis. In our case, only the casing-shoe area was taken into account. The effects of the parameters on the stability of salt rock around the casing-shoe area were examined for the cavern depth, cavern shape, cavern volume, minimum and maximum pressure gradients, cycling number, cycling period, and gas injection temperature.

Table 7. Parameters considered for the sensitivity analysis.

Type	Check effect	Unit	Range					
			Baseline					
Geometry	Cavern depth	m		500	1000	1500		
	Cavern shape	H:D ratio		1	3	5	7	9
	Cavern volume	$\times 10^5$ m^3		4	8			
Operational	Min pressure	psi/ft			0.2	0.3	0.4	
	Max pressure	psi/ft	0.75	0.80	0.85			
	Cycle's number	-			10	20		
	Cycle's period	Day	30	180	365			
	Gas injection temperature	˚C		21	37	54		

Earlier caverns had a geometric volume less than 100,000 m^3 but the recent caverns have been designed and constructed with a geometric storage volume of more than 10^6 m^3. Gas storage cavern depth covers a wide range from 500 m to more than 1500 m with compact to slim cavities in shape. The need for improved economic benefits changes the operation pattern of gas storage cavities from seasonal storage to a frequent turnover. Each one of the baseline parameters was varied to determine the effect of the parameter involved on the stability criteria for salt rock around the casing-shoe area.

Table 8 shows the correlation between the parameters and their impact on the stability of salt rock in the casing-shoe area with respect to the stability criteria (including no tension, no effective tension, dilation, and cavern loss volume rate). An upward pointing arrow (↑) indicates an advantageous impact; a downward pointing arrow (↓) indicates a disadvantageous impact. We can obtain useful clues in Table8 for the geometrical and operational parameters by anticipating the degree to which the parameters impact the stability of salt rock in the casing-shoe area and cavern volume-loss rate.

Considering the cavern volume-loss rate, the cavern depth and minimum pressure, among other parameters, have the largest impact on the rate of cavern volume-loss. As expected, increasing the cavern depth will result in an increase in the cavern volume-loss rate. The reverse is true when the minimum pressure increases.

The first baseline parameter evaluated was the cavern depth. In these simulations, the average depth of the cavern was varied from 500 m to 1,500 m, which had a very significant impact on the cavern stability. Increasing the cavern depth increases the tensile stresses at the casing-shoe but it also reduces the potential of developing effective tensile stresses and dilation.

As shown in Table 8, the minimum gas pressure has a large impact on the cavern stability at the casing-shoe area. Lowering the minimum gas pressure not only increases the development of tensile stresses but also increases the dilation potential in the vicinity of the casing-shoe. In contrast to the minimum gas-pressure effect, the maximum gas-pressure changes have a limited impact on the stability of salt rock at the casing-shoe area.

The next parameter evaluated was the cavern shape, which was introduced with a height-to-diameter (H/D) ratio. Increasing the H/D ratio has a positive impact on the stability of salt rock at the casing-shoe area. In other words, the slim cavern is more stable than the others. It should be noted that in this work, the pressure gradients were assumed to remain at the baseline values of depth at the casing seat. Thus increasing the H/D ratio will result in a decreased value of pressure in the cavern.

Increasing the number of operation cycles from 10 to 20 develops tensile stress and tensile effective stress at the casing-shoe area.

Increasing the cycling period from 30 days (12 cycles per year) to 365 days (1 cycle per year) increases the development of tensile and effective tensile stresses and reduces dilation potential at the casing-shoe area.

The last parameter considered was the gas-injection temperature. Variations in this temperature had a very limited impact on the stability of salt in the casing-shoe area.

Table 8. Correlation table: (↑): Advantage, (↓): Disadvantage.

Type	Check effect	Stability Criteria			
			at the Casing-shoe Area		
		Volume loss rate (% per year)	Least compress stress	Effective stress	Dilation (DV)
Geometry	Cavern depth (↑)	(↑) VH	(↑) VH	(↓) H	(↓) VH
	Cavern shape (↑)	(↓) L	(↑) L	(↑) L	(↑) H
	Cavern volume (↑)	(↓) VL	(↓) VL	(↓) VL	(↓) H
Operational	Min pressure (↑)	(↑) VH	(↑) VH	(↑) L	(↑) H
	Max pressure (↑)	(↑) L	NE	(↓) L	NE
	Cycle's number (↑)	NE	(↓) L	(↓) L	NE
	Cycle's period (↑)	(↓) L	(↓) L	(↓) VL	(↑) L
	Gas injection temperature (↑)	(↓) VL	(↓) VL	(↑) VL	NE

NE: No measurable effect, VL: very low, L: low, H: high, VH: very high.

5. Conclusions

This paper presents the results of a coupled thermo-hydro-mechanical modeling study that was performed to identify the roles of the geometrical and operational factors on the stability of a solution-mined gas storage cavern. Totally, four criteria including (1) least principal-stress, (2) effective stress (3) dilation situations around the cavern, and (4) cavern volume loss rate were applied to investigate the stability and serviceability of a single cavern by means of a 2D THM finite element program (LOCAS). Also an advanced rock salt constitutive model (MD model) was utilized to simulate the behavior of the surrounding salt formation of the proposed cavern during leaching, first gas filling, and cyclic operational phases. First, a baseline capsule-shape cavern was built, and all the stability criteria were examined along the cavern periphery and also in the surrounding salt. After that, a sensitivity analysis was carried out to evaluate the influences of the most important geometrical and operational parameters on the cavern stability.

Regarding the temperature profile of the gas in the baseline cavern, the results obtained showed that the gas temperature fluctuated in the order of 20-30 degrees between the max and min peaks during the operational phase. This significant temperature change might be triggered with the development of temperature-induce stresses in the vicinity of the salt cavern walls.

The trend of cavern volume-loss rate of the proposed baseline cavern illustrateed that the cavern suffered a very rapid volume-loss rate during the first cycle, where the gas pressure reached its minimum value.

Also the results of this work showed that dilation was more likely to occur during the first cycle of the cavern life when the pressure dropped to the minimum. The potential of tension in the surrounding rocks is more likely to occur when the number of cycles increases, especially at the upper part of the cavern wall. When considering a long period of time, due to the viscose characteristics of salt, a decrease in the deviatoric stress could be observed. Also the cavern volume-loss rate for the baseline model was within the acceptable range.

Following the baseline model examination, numerous 2D axisymmetric finite element numerical models were developed to check the effects of the geometrical and operational factors on the structural stability of gas caverns in the casing-shoe area and on the cavern volume-loss rate. The results of the sensitivity study indicated that the two factors minimum pressure and cavern depth had the largest impact on the stability of rock salt at the casing-shoe area.

In our case, different operational scenarios with different withdrawal and injection rates and periods were described and discussed. Other scenarios include an idle time period under maximum or minimum pressure that may seem more practical, and they were not considered in this work, where only a single cavern was assumed and the nearby caverns were not explicitly modeled.

Acknowledgments

This work was funded by the National Iranian Gas Company (NIGC) under the contract No. 190081. We also would like to express our sincere appreciation to the Natural Gas Storage Company (NGSC) for their supports.

References

[1]. Minkley, W., Lindert, A. and Brückner, D. (2011). The improved IfG Gas Storage Cavern Design

Concept, in SMRI Fall 2011 Technical Conference. York, United Kingdom.

[2]. Réveillère, A., Bérest, P., Evans, D.J., Stöwer, M., Chabannes, C., Koopmans, T. and Bolt, R. (2017). Past salt caverns incidents database Part 1 leakage, overfilling and blowout.

[3]. Staudtmeister, K. and Zapf, D. (2010). Rock Mechanical Design of Gas Storage Caverns for Seasonal Storage and Cyclic Operations, in SMRI Spring 2010 Technical Conference. Grand Junction, Colorado, USA.

[4]. Lestringant, C., Bérest, P. and Brouard, B. (2010). Thermo-mechanical effects in compressed air storage (CAES), in SMRI Fall 2010 Technical Conference. Leipzig, Germany.

[5]. Lux, K.H.(2009). Design of salt caverns for the storage of natural gas, crude oil and compressed air: Geomechanical aspects of construction, operation and abandonment, Underground Gas Storage, Evans D.J. & Chadwick R. A, Editor. p. 93-128.

[6]. Pudewills, A. (2012). Numerical simulation of coupled Thermo-Hydro-Mechanical processes in rock salt, in 7th conference on the Mechanical Behavior of Salt. Paris, France.

[7]. Liu, J. and Xiao, Q. (2014). The Influence of Operation Pressure on the Long-Term Stability of Salt-Cavern Gas Storage. Advances in Mechanical Engineering. **6**: p. 537679.

[8]. Li, M., Hou, Z., Li, M., Gou, Y. and Tao, S. (2018). Numerical study of a novel two-well horizontal gas storage cavern in thin-bedded rock salt in China, in Mechanical Behavior of Salt iX. CRC Press. p. 911-923.

[9]. Ghasemloonia, A and Butt, S.D. (2015). Feasibility study of underground salt caverns in Western Newfoundland: experimental and finite element investigation of creep-induced damage. Journal of Mining and Environment. **6** (2): p. 205-224.

[10]. Heusermann, S., Rolfs, O. and Schmidt, U. (2003). Nonlinear finite-element analysis of solution mined storage caverns in rock salt using the LUBBY2 constitutive model. Computers & structures. **81** (8-11): p. 629-638.

[11]. Reedlunn, B. (2018). Joint Project III on the Comparison of Constitutive Models for the Mechanical Behavior of Rock Salt: Reinvestigation into Isothermal Room Closure Predictions at the Waste Isolation Pilot Plant, in Mechanical Behavior of Salt iX. CRC Press. p. 447-458.

[12]. Hampel, A., Salzer, K., Günther, R.M., Minkley, W., Pudewills, A., Leuger, B., Zapf, D., Staudtmeister, K., Rokahr, R. and Herchen, K. (2012). Joint Projects on the Comparison of Constitutive Models for the Mechanical Behavior of Rock Salt-II. Overview of the models and results of 3-D benchmark calculations, in Mechanical Behaviour of Salt VII. CRC Press. p. 245-254.

[13]. Hampel, A., Günther, R.M., Salzer, K., Minkley, W., Pudewills, A., Yildirim, S., Rokahr, R.B., Gährken, A., Missal, C. and Stahlmann, J. (2015). Joint Project III on the comparison of constitutive models for the thermo-mechanical behavior of rock salt I–Overview and results from model calculations of healing of rock salt. Roberts, Mellgard & Hansen (eds) Mechanical Behaviour of Salt VIII. London.

[14]. Khaledi, K. (2017). Constitutive modeling of rock salt with application to energy storage caverns. Ruhr-Universit at Bochum, Faculty of Civil and Environmental Engineering: Bochum.

[15]. Lux, K.H. and Düsterloh, U. (2015). From birth to long-term life—main aspects regarding THM-coupled simulation of salt cavern behavior as well as regarding improved salt cavern design with special consideration of rock salt damage, in Mechanical Behaviour of Salt VIII. CRC Press. p. 285-302.

[16]. Asgari, A., Ramezanzadeh, A., Jalali, S.M.E. and Brouard, B. (2014). Impact of Geomechanical Parameters on Stability of Natural Gas Storage Salt Caverns, in 5th Iranian Rock Mechanics Conference (IRMC5) Tehran, Iran.

[17]. Hirth, J.P. and Lothe, J. (1982). Theory of dislocations.

[18]. Khaledi, K., Mahmoudi, E., Datcheva, M. and Schanz, Tom. (2016). Stability and serviceability of underground energy storage caverns in rock salt subjected to mechanical cyclic loading. International journal of rock mechanics and mining sciences. **86**: p. 115-131.

[19]. Munson, D.E. and Dawson, P.R. (1981). Salt-constitutive modeling using mechanism maps. Sandia National Labs.

[20]. Argüello, J.G. and Holland, J.F. (2015). Two problems to benchmark numerical codes for use in potential HLW salt repositories: J. Guadalupe Argüello & JF Holland, in Mechanical Behaviour of Salt VIII. CRC Press. p. 373-384.

[21]. Costa, A.M., Costa, P.V.M., Amaral, C.S. and Poiate J.E. (2015). Computer modeling applied in the design of salt caverns for natural gas storage: AM Costa PVM Costa, in Mechanical Behaviour of Salt VIII. CRC Press. p. 277-284.

[22]. Firme, P., Roehl, D., Romanel, C., Poiate J.E. and Costa, A.M. (2015). Multi-mechanism deformation creep model applied to Brazilian salt rocks: PALP Firme D. Roehl, in Mechanical Behaviour of Salt VIII. CRC Press. p. 351-358.

[23]. Schulze, O., Heemann, U., Zetsche, F., Hampel, A., Pudewills, A., Günther, R.M., Minkley, W., Salzer, K., Hou, Z. and Wolters, R. (2007). Comparison of advanced constitutive models for the mechanical

behavior of rock salt-results from a joint research project. I. Modeling of deformation processes and benchmark calculations, in Proc. of the 6th Conf. on the Mech. Behaviour of Salt (Eds.: Wallner, M., Lux, K.-H., Minkley, W. & Hardy, Jr., HR), Hannover. p. 77-88.

[24]. Hampel, A., Gunther, R.M., Salzer, K., Minkley, W., Pudewills, A., Leuger, B., Zapf, D., Staudtmeister, K., Rokahr, R. and Herchen, K. (2010). Benchmarking of geomechanical constitutive models for rock salt, in 44th US Rock Mechanics Symposium and 5th US-Canada Rock Mechanics Symposium. American Rock Mechanics Association.

[25]. Leuger, B., Staudtmeister, K., Yıldırım, S. and Zapf, D. (2010). Modeling of creep mechanism and damage of rock salt, in 7th European Conference on Numerical Methods in Geotechnical Engineering (NUMGE 2010), 02–04 June 2004, Trondheim/Norway. p. 89-94.

[26]. Costa, A.M., Costa, P.V.M., Ruggeri, F., Ebecken, N.F.F., Miranda, A.C.O., Nishimoto, K., Meneghini, J.R., Eston, S.M., Tomi, G., Brandão, C. and Breda, A. (2018). Salt Rock, a Strategic Geomaterial in Brazil, in Mechanical Behavior of Salt iX. CRC Press. p. 855-870.

[27]. Pedro, A., Firme, L.P., Roehl, D. and Romanel, C. (2018). A glance into the mechanical behavior of salt caverns towards future natural gas strategic storage in Brazil, in Mechanical Behavior of Salt iX. CRC Press. p. 843-854.

[28]. Brouard, B., Zakharov, V., Frangi, A. and Cremonesi, M. (2018). Introducing LOCAS 3D Application to the Geomechanical Modeling of an Oil-Storage Facility, in SMRI Fall 2018 Conference. Belfast, Northern Ireland, UK.

[29]. Brouard, B., Berest, P. and Durup, G. (2002). LOCAS: A first salt cavern abandonment software, in SMRI Spring Conference 2002. Banff, Alberta, Canada.

[30]. Brouard, B., Karimi-Jafari, M., Bérest, P. and Frangi, A. (2006). Using LOCAS software to better understand the behavior of salt caverns, in SMRI Spring Meeting. Brussels, Belgium. p. 273-288.

[31]. Brouard, B., Karimi-Jafari, M., Bérest, P. and Durup, G. (2007). Pressure Build-up in a Sealed Cavern: he Effect of a Gas Blanket, in SMRI Spring 2007 Conference. Basel, Switzerland.

[32]. Karimi–Jafari, M., Gatelier, N., Brouard, B., Bérest, P. and Djizanne, H. (2011). Multi-cycle gas storage in salt caverns, in SMRI 2011 Conference. York, United Kingdom.

[33]. Djizanne, H., Bérest, P. and Brouard, B. (2014). The Mechanical Stability of a Salt Cavern Used for Compressed Air Energy Storage (CAES), in SMRI Spring 2014 Conference. San Antonio, Texas.

[34]. Djizanne, H., Bérest, P., Brouard, B. and Frangi, A. (2014). Blowout in gas storage caverns. Oil & Gas Science and Technology–Revue d'IFP Energies nouvelles. **69.**(7): p. 1251-1267.

[35]. Brouard, B., Frangi, A. and Bérest, P. (2011). Mechanical Stability of a Cavern Submitted to High-Frequency Cycles, in SMRI Spring 2011 Technical Conference. Galveston, Texas, USA.

[36]. Brouard, B., Bérest, P. and Frangi, A. (2018). Failure mechanisms in a cycled gas cavern, in Mechanical Behavior of Salt iX. CRC Press. p. 791-805.

[37]. Devries, K.L., Mellegard, K.D. and Callahan, G.D. (2002). Salt damage criterion proof-of-concept research. Respec, Inc.(US).

[38]. Nieland, J.D. (2008). Salt cavern Thermodynamics-Comparison Between Hydrogen, Natural Gas and Air Storage. , in SMRI Fall Meeting. Austin, Texas. p. 215-234.

[39]. Costa, A.M., Amaral, C.S., Poiate, E., Quispe, R.J.Q., Morales, M.S.T. and Roehl, D. (2015). Sensitivity study of the finite element modeling applied in the closure analysis of the pre-salt wells in Brazil, in Mechanical Behavior of Salt VIII. CRC Press. p. 425-432.

[40]. Devries, K.L., Mellegard, K.D., Callahan, G.D. and Goodman, W.M. (2005). Cavern roof stability for natural gas storage in bedded salt. RESPEC.

[41]. Lux, K.H., Wolters, R., Feierabend, J., Pan, T. and Rutenberg, M. (2018). Fluid dynamic processes within a closed repository in rock salt mass without or with additional components for long-term monitoring, in Mechanical Behavior of Salt iX. CRC Press. p. 663-677.

[42]. Brouard, B. and Nieland, J.D. (2013). Analysis of Moss Bluff Cavern Blowout Data SOLUT ION MINING RESEARCH INSTITUTE, RESEARCH REPORT 2013-01.

[43]. Hou, Z. and Lux, K.H., (2004) A new coupling concept for the hydro-mechanical interaction of clay stone and rock salt in underground waste repositories. International Journal of Rock Mechanics and Mining Sciences. **41**: p. 708-713.

[44]. Durup, J.G., Vidal, F. and Rolin, C., (2007) Pilot abandonment test of a very deep gas storage salt cavern. Oil & Gas Science and Technology-Revue de l'IFP. **62** (3): p. 287-296.

[45]. Spiers, C.J., Peach, C.J., Brzesowsky, R.H., Schutjens, P.M.T.M., Liezenberg, J.L. and Zwart, H.J. (1988). Long-term rheological and transport properties of dry and wet salt rocks. Commission of the European Communities.

[46]. Ratigan, J.L., Van Sambeek, L.L., Devries, K.L. and Nieland, J.D. (1991). The influence of seal design

on the development of disturbed rock zone in the WlPP alcove seal test. Rep. RSI-0400, RE/SPEC Inc.,Rapid City, S. D.

[47]. Hunsche, U.E. (1993). Failure behaviour of rock salt around underground cavities, in Proceedings of the 7th Symposium on Salt. p. 59-65.

[48]. Thorel, L., Ghoreychi, M., Cosenza, P. and Chanchole, S. (1996). Rocksalt damage and failure under dry or wet conditions, in 4th conference on the mechanical behavior of salt, Montréal (Canada). p. 189–202.

[49]. Hatzor, Y.H. and Heyman, E.P. (1997). Dilation of anisotropic rock salt: Evidence from Mount Sedom diapir. Journal of Geophysical Research: Solid Earth. **102** (B7): p. 14853-14868.

[50]. Hampel, A. (2012). The CDM constitutive model for the mechanical behavior of rock salt: Recent developments and extensions, in Proceedings of the 7th Conference on Mechanical Behaviour of Salt, Paris. p. 16-19.

تحلیل پایداری مغار نمک ذخیره‌ساز گاز طبیعی با در نظر گرفتن شرایط فرآیندهای توامان هیدرو-ترمومکانیکی و استفاده از یک نرم افزار المان محدود دو بعدی

امین عسگری[1*]، احمد رمضان‌زاده[1]، سید محمداسماعیل جلالی[1] و بنوآ بروآرد[2]

1- دانشکده مهندسی معدن، ژئوفیزیک و نفت، دانشگاه صنعتی شاهرود، ایران

2- شرکت مهندسین مشاور بروآرد، پاریس، فرانسه

ارسال 2019/04/27، پذیرش 2019/11/14

* نویسنده مسئول مکاتبات: Amin.Asgari@shahroodut.ac.ir

چکیده:

پایداری مکانیکی و استحکام هیدرولیکی مغارهای نمک ذخیره‌ساز گاز طبیعی تحت اثر رفتار غیر خطی و وابسته به زمان سنگ نمک ناشی از شرایط بارگذاری پیچیده ترمومکانیکی وارد برآن است. به همین دلیل، ابزارهای عددی مورد استفاده در تحلیل چنین شرایطی باید قادر باشند اثر نوسانات فشار و دمای درون مغار را بر سازند نمک دربرگیرنده آن بخوبی مدل نمایند.در این پژوهش از نرم افزار LOCAS، که یک کد دو بعدی المان محدود بوده که فقط به صورت انحصاری جهت تحلیل پایداری مغارهای نمک توسعه یافته، به منظور ارزیابی نحوه تاثیر پارامترهای بهره‌برداری و هندسی مغار مورد استفاده قرار گرفته است. به طور کلی هدف پژوهش حاضر، ایجاد درک کلی از رفتار مغارهای نمکی است که با مقاصد ذخیره‌سازی گاز طبیعی مورد استفاده قرار می‌گیرند. روش کار در این پژوهش بدین ترتیب است که ابتدا سناریوهای بارگذاری مشخصی در نظر گرفته شده و سپس با استفاده از تحلیل‌های پارامتری و تحلیل حساسیت، نحوه تاثیر پارامترهای هندسی و بهره‌برداری مغار نمک با توجه به معیارهای پایداری مورد ارزیابی قرار گرفته‌اند. نتایج این پژوهش نشان می‌دهد که احتمال اتساع دیواره نمک مغار در چرخه‌های ابتدایی فرآیند بهره‌برداری و در زمانی که فشار گاز درون مغار به حداقل میزان خود می‌رسد، بیش از سایر زمان‌ها است. همچنین پتانسیل وقوع شرایط کششی جداره مغار به خصوص در یک سوم بالایی آن با افزایش تعداد چرخه‌های بهره‌برداری دائماً افزایش می‌یابد. در نهایت چنین نتیجه‌گیری شد که دو پارامتر عمق قرارگیری مغار و میزان فشار داخلی حداقلی مغار نسبت به سایر پارامترها اثر بزرگتری بر نحوه رفتار مغار نمک از خود نشان می‌دهند.

کلمات کلیدی: مغار نمک، تحلیل پایداری، مدل‌سازی المان محدود، تحلیل حساسیت.